Urban aerosol chemistry at a land-water transition site during summer – Part 2: Aerosol pH and liquid water content

Michael A. Battaglia, Jr.[1,a], Nicholas Balasus[1], Katherine Ball[1], Vanessa Caicedo[2], Ruben Delgado[2], Annmarie G. Carlton[3] , and Christopher J. Hennigan[1*]

[1]Department of Chemical, Biochemical, and Environmental Engineering, University of Maryland, Baltimore County

[2]Joint Center for Earth Systems Technology, University of Maryland, Baltimore County

[3]Department of Chemistry, University of California, Irvine

[a]Current affiliation: School of Earth and Atmospheric Sciences, Georgia Institute of Technology

Correspondence: C. J. Hennigan (hennigan@umbc.edu)

1 **Abstract**
2
3   Particle acidity (aerosol pH) is an important driver of atmospheric chemical processes

4 and the resulting effects on human and environmental health. Understanding the factors that

5 control aerosol pH is critical when enacting control strategies targeting specific outcomes. This

6 study characterizes aerosol pH at a land-water transition site near Baltimore, MD during summer

7 2018 as part of the second Ozone Water-Land Environmental Transition Study (OWLETS-2)

8 field campaign. Inorganic fine mode aerosol composition, gas-phase NH_3 measurements, and all

9 relevant meteorological parameters were used to characterize the effects of temperature, aerosol

10 liquid water (ALW), and composition on predictions of aerosol pH. Temperature, the factor

11 linked to the control of NH_3 partitioning, was found to have the most significant effect on aerosol

12 pH during OWLETS-2. Overall, pH varied with temperature at a rate of -0.047 K^{-1} across all

13 observations, though the sensitivity was -0.085 K^{-1} for temperatures > 293 K. ALW had a minor

14   effect on pH, except at the lowest ALW levels (< 1 μg m^{-3}) which caused a significant increase

15   in aerosol acidity (decrease in pH). Aerosol pH was generally insensitive to composition (SO_4^{2-},

16   SO_4^{2-}:NH_4^+, Tot-NH$_3$ = NH$_3$ + NH$_4^+$), consistent with recent studies in other locations. In a

17   companion paper, the sources of episodic NH$_3$ events (95th percentile concentrations, NH$_3$ > 7.96

18   μg m^{-3}) during the study are analyzed; aerosol pH was higher by only ~0.1-0.2 pH units during

19   these events compared to the study mean. A case study was analyzed to characterize the

20   response of aerosol pH to nonvolatile cations (NVCs) during a period strongly influenced by

21   primary Chesapeake Bay emissions. Depending on the method used, aerosol pH was estimated

22   to be either weakly (~0.1 pH unit change based on NH$_3$ partitioning calculation) or strongly

23   (~1.4 pH unit change based on ISORROPIA thermodynamic model predictions) affected by

24   NVCs. The case study suggests a strong pH gradient with size during the event and underscores

25   the need to evaluate assumptions of aerosol mixing state applied to pH calculations. Unique

26   features of this study, including the urban land-water transition site and the strong influence of

27   NH$_3$ emissions from both agricultural and industrial sources, add to the understanding of aerosol

28   pH and its controlling factors in diverse environments.

1 Introduction

The acidity, or pH, of atmospheric aerosols affects the chemical and physical properties of airborne particles, and thus, their impacts on climate and health (Pye et al., 2020). The gas-particle partitioning of semi-volatile acidic and basic compounds – notably NH_3, HNO_3, HCl, and organic acids – depends in part on aerosol pH, which directly affects the particulate matter (PM) mass concentration (Nenes et al., 2020). The solubility of many particulate components is pH-dependent, including metals and nutrients, with implications for particle toxicity and nutrient deposition to ecosystems (Fang et al., 2017; Kanakidou et al., 2016). The optical properties of light-absorbing organic compounds, known as brown carbon, can exhibit a strong pH-dependence, which directly affects their climate impacts (Phillips et al., 2017). However, direct measurements of aerosol pH remain challenging. Single particle studies of aerosol pH using Raman spectroscopy have been performed, but are limited by the presence of both HSO_4^- and SO_4^- limiting their application to more acidic particles (Boyer et al., 2020; Rindelaub et al., 2016). Colorimetric measurements of aerosol pH have also been employed, but such techniques have been limited to laboratory studies with relatively simple aerosol compositions (Craig et al., 2018); (Jang et al., 2020). Given the importance of aerosol pH for atmospheric processes and the limitation in estimating acidity with proxies (e.g., ion balances), there has been increased effort in recent years to identify the factors that affect pH and to characterize temporal and spatial variations in the atmosphere (Hennigan et al., 2015).

Globally, aerosol pH is often quite acidic due to the ubiquity and abundance of strong acids like H_2SO_4, HNO_3, and HCl (Pye et al., 2020). Ammonia (NH_3) is unique among species that affect pH because it is the most abundant basic compound in the atmosphere. NH_3 partitioning is controlled by the concentration of strong acids and by the ambient temperature

53   and relative humidity, hence, the dependence of pH on both composition and meteorology

54   (Zheng et al., 2020). In some regimes, the meteorological factors are more important than the

55   compositional factors, explaining why NH_3 can exist partially in the gas phase even when the

56   aerosol pH is highly acidic (Nenes et al., 2020; Weber et al., 2016). Due to its abundance and

57   semi-volatile properties, NH_3 was identified as the most important buffering agent in aerosols

58   across locations with diverse emissions, composition, and climatology (Zheng et al., 2020). In

59   single-phase aqueous particles, organic compounds have a minor effect on pH (Battaglia Jr et al.,

60   2019), though this is not the case for particles that have undergone liquid-liquid phase separation

61   (Pye et al., 2018). Non-volatile cations (NVC) typically contribute a minor fraction of PM mass

62   but can be critical for accurate predictions of pH, especially if NVC concentrations are

63   overestimated (Vasilakos et al., 2018). Globally, NVC are most important in regions heavily

64   impacted by dust emissions (Pye et al., 2020), but have minor effects on pH in other regions (Tao

65   & Murphy, 2019; Zheng et al., 2020).

66   Aerosol pH is also strongly affected by meteorological factors. Equilibrium constants,

67   including those that determine the gas-particle partitioning and aqueous dissociation of semi-

68   volatile acids and bases, are temperature dependent. Temperature is a dominant factor driving

69   variability in the seasonal and diurnal cycling of pH (Guo et al., 2015; Tao & Murphy, 2019).

70   Temperature gradients, as occur in and around urban areas, can also drive large differences in

71   pH, even if the composition is uniform over the same scales (Battaglia et al., 2017). Relative

72   humidity (RH) regulates aerosol liquid water content (ALWC), which affects the partitioning of

73   soluble gases and aqueous phase solute concentrations. ALWC may be the most important

74   factor responsible for large pH differences observed between the southeast US (pH ~0.5-1.0) and

75   the heavily polluted North China Plain (pH ~4-5), the two regions where pH has been most

76 extensively studied to-date (Zheng et al., 2020). These effects can be complex, or even partially

77 offset. For example, an increase in temperature reduces pH owing to the shift in NH_3

78 partitioning towards the gas phase, but NH_3 emissions increase with temperature as well,

79 producing an increase in pH and partially offsetting the pH changes due to temperature (Tao,

80 2020). More research is needed to better understand how all these factors together affect pH, and

81 how this changes geographically and temporally.

82   In this study aerosol pH was characterized during the summertime (4 June to 5 July,

83 2018) at a land-water transition site near a large urban area (Baltimore, MD) as part of the

84 OWLETS-2 (second Ozone Water-Land Environmental Transition Study) field campaign. This

85 site is unique because meteorological phenomena, such as the bay breeze, affect pollution

86 dispersion and recirculation (Loughner et al., 2014). Baltimore is impacted by different regional

87 emission sources, as it is located in the populous and heavily trafficked I-95 corridor, downwind

88 of the Ohio River Valley (He et al., 2013), and relatively close to regional agricultural operations

89 that emit large amounts of NH_3 (Pinder et al., 2006). In a companion paper, the local sources of

90 NH_3 during the OWLETS-2 study were examined, including an analysis of transient events with

91 unexpectedly high NH_3 concentrations (Balasus et al., 2021). In this study, the effects of the

92 observed NH_3 concentrations (including the aforementioned transient concentrations of

93 unexpectedly high values), in combination with the unique meteorological phenomena associated

94 with the land-water transition, on ALW and aerosol pH were investigated.

95

96 **2 Methods**

97   The OWLETS-2 study was conducted to characterize effects of meteorological

98 phenomena associated with the land-water transition on summertime air quality in Baltimore.

99   Hart-Miller Island (HMI, coordinates 39.2421°, -76.3627°), a site located on the Chesapeake Bay

100   ~10 km east of downtown Baltimore, hosted many of the ground-based measurements during the

101   study (Fig. S1). Semi-continuous measurements of aerosol inorganic chemical composition and

102   gas-phase NH_3 were conducted at HMI. The measurement details are provided in the companion

103   paper (Balasus et al., 2021). Briefly, the water-soluble ionic components of $PM_{2.5}$ were

104   measured with a Particle-into-Liquid Sampler coupled to a dual Ion Chromatograph (PILS-IC,

105   Metrohm) operated according to Valerino et al. (2017). NH_3 was measured with an AiRRmonia

106   Analyzer (RR Mechatronics) (Norman et al., 2009). Meteorological parameters were measured

107   with a Vaisala MAWS201 Met Station at 1-minute resolution.

108   The 5-minute NH_3 measurements and 1-minute meteorological measurements were

109   averaged to the 20-mintue sampling time of the PILS-IC. Aerosol pH for each 20-min sample

110   was calculated according to the NH_3 partitioning method presented in Zheng et al. (2020). This

111   method uses the relevant temperature-dependent equilibrium constants and the measured

112   concentrations of NH_3 and NH_4^+ to calculate pH. The method of Zheng et al. (2020) is based

113   upon a similar approach in prior studies (Hennigan et al., 2015; Keene et al., 2004); the two

114   methods are identical, with minor differences only due to equilibrium constant values used based

115   on ranges provided in the literature. Indeed, very close agreement was observed (slope = 0.967,

116   R^2 = 0.977, n = 872) in calculated pH between the NH_3 partitioning methods of Zheng et al.

117   (2020) and Hennigan et al. (2015). The aqueous phase NH_4^+ concentration is derived from the

118   mass concentration of NH_4^+ from the PILS-IC and the ALWC. The ISORROPIA-II

119   thermodynamic equilibrium model was used to calculate ALWC using the PILS-IC, NH_3, and

120   meteorological data as inputs (Fountoukis & Nenes, 2007). The model was run in forward mode

121   (NH_3 and aerosol NH_4^+ were input at total NH_3) using the metastable assumption according to

122   the recommendation of Guo et al. (2015).

123   Although ISORROPIA can provide pH, the NH_3 partitioning method was used for pH

124   calculations in this study:

$$125 \qquad pH = pK_{a,NH_3}^* + log_{10} \frac{[NH_3(aq)] + [NH_3(g)]}{[NH_4^+(aq)]} \qquad (1)$$

$$126 \qquad [NH_3(g)] = \frac{p_{NH_3}\rho_w}{RT\ AWC} \qquad (2)$$

$$127 \qquad K_{a,NH_3}^* = \frac{[H^+(aq)]([NH_3(aq)] + [NH_3(g)])}{[NH_4^+(aq)]} = K_{a,NH_3}\left(1 + \frac{\rho_w}{H_{NH_3}RT\ AWC}\right) \qquad (3)$$

128   where in Equation 1, $[NH_3(aq)]$ is the molality of NH_3 in solution (mol kg^{-1}, calculated by

129   multiplying H_{NH_3} and p_{NH_3}), $[NH_3(g)]$ is the equivalent molality of gaseous NH_3 in solution

130   (mol kg^{-1}, given by Equation 2), and $[NH_4^+(aq)]$ is the molality of NH_4^+ in solution (mol kg^{-1}).

131   Equation 2 calculates $[NH_3(g)]$, where p_{NH_3} is the partial pressure of NH_3 (atm), ρ_w is the

132   density of water (μg m^{-3}), R is the gas constant (atm L mol^{-1} K^{-1}), T is temperature (K), and

133   AWC is aerosol water content (μg m^{-3} air). Equation 3 calculates the last unknown term in

134   Equation 1, which is K_{a,NH_3}^*, the effective dissociation constant (where H_{NH_3} is the Henry's law

135   constant of NH_3 in mol kg^{-1} atm^{-1}).

136   Direct measurements of aerosol pH are not available to test model predictions so the

137   partitioning of semi-volatile species that depend on pH, most commonly NH_3/NH_4^+ and

138   HNO_3/NO_3^-, is a key metric used to evaluate model performance (Pye et al., 2020).

139   ISORROPIA is used extensively for predictions of pH; however, in this study the measured and

140   ISORROPIA-predicted values of NH_3 partitioning (ε_{NH3} = $NH_3/(NH_3 + NH_4^+)$) did not always

141   agree well (Fig. S2). There were systematic differences in pH between the two methods (mean

142   pH difference = 0.6 pH units), and they were not correlated (R^2 = 0.097, not shown). The source

143   of the discrepancy in NH_3 partitioning (ISORROPIA modeled versus measurement-calculated) is

144   unknown, though it is not likely the result of an incorrect assumption of equilibrium (see the SI

145   and the companion paper Balasus et al. (2021) for more details).

146   Commonly, a reasonable estimate of measurement errors associated with the species of

147   interest are on the order of 15% + 1 nmol m^{-3} for online sampling methods (Murphy et al., 2017).

148   Utilizing this estimate in the extreme acidic case (ambient observed SO_4^{2-} and NO_3^- adjusted to +

149   15% + 1 nmol m^{-3}; NH_4^+ adjusted to – 15% – 1 nmol m^{-3}) or non-acidic case (SO_4^{2-} and NO_3^-

150   adjusted down by – 15% – 1 nmol m^{-3} and NH_4^+ adjusted up by + 15% + 1 nmol m^{-3}), the

151   uncertainty of aerosol pH was predicted to vary by 0.1 – 1 pH units (Murphy et al. 2017).

152   Similarly, Pye et al. (2020) reported that in cases for RH above 60%, deviations of the

153   ISORROPIA-predicted pH and the IUPAC-defined pH are less than one pH unit. The present

154   calculations have similar uncertainties in the pH calculations.

155

156   **3 Results and Discussion**

157   **3.1 Meteorological effect on pH**

158   As in many cities, the urban heat island effect in Baltimore evolves throughout the day,

159   with urban-rural temperature and RH gradients peaking at night (Battaglia et al., 2017).

160   Meteorological conditions at HMI demonstrate unique features associated with the land-water

161   transition. At night, the average temperature observed at HMI was close to conditions observed

162   in downtown Baltimore but transitioned to match the conditions at a nearby rural site during the

163   day (Fig. 1a). Overall, the range in average hourly temperatures at HMI was lower (4.3 °C; 22.5

164   – 26.8 °C) than the averages observed at either the downtown site (range 6.2 °C; 22.8 – 29.0 °C)

165   or the rural site (range 8.8 °C; 17.5 – 26.3 °C). Likewise, the average hourly RH profile at HMI

166 had a significantly smaller range (13.7%; 61.7 – 75.4%) than the RH profiles at the downtown

167 (range 22.1%; 53.2 – 75.3%) or rural sites (range 30.3%; 55.9 – 86.2%) (Fig. 1b). The

168 differences shown in Fig. 1 were due to the proximity of HMI to the Chesapeake Bay and have

169 several implications for aerosol pH, which will be discussed in detail below.

170   Due to the meteorological conditions discussed above, the diurnal profile of ALWC at

171 HMI was unique (Fig. 2a). Typical profiles of ALWC in the eastern US closely follow RH, with

172 minima in the afternoon and maxima at night or in the pre-dawn morning hours (Guo et al.,

173 2015; Battaglia et al., 2017). During OWLETS-2, ALWC did not show a distinct diurnal profile

174 that was correlated with RH. Instead, the highest median ALWC at HMI occurred between

175 12:00 – 14:00, (local time, LT; during the study this is UTC-4) (Fig. 2a). This daily peak in

176 ALWC coincided with a pronounced enhancement in aerosol NO_3^-, which is discussed in the

177 companion paper (Balasus et al., 2021). The partitioning of NH_3, ε_{NH3}, also showed a diurnal

178 profile that was unexpected (Fig. 2b). Due to the strong temperature dependence of vapor

179 pressure and equilibrium constants, NH_3 partitioning typically shifts towards the gas-phase

180 during the daytime (ε_{NH3} increases) and shifts towards the aerosol phase at night (ε_{NH3} decreases)

181 (Guo et al., 2017). The increase in gas-phase NH_3 emissions with increasing temperature can

182 also contribute to an elevated ε_{NH3} during the daytime. The diurnal profile of ε_{NH3} observed at

183 HMI did not follow temperature, as the median ε_{NH3} peaked during the 06:00 – 08:00 LT, and

184 decreased slightly into the afternoon (Fig. 2b). This shows a shift of NH_3 partitioning towards

185 the condensed phase as daily temperatures peaked. This was enabled by the ALWC remaining

186 steady throughout the afternoon. Overall, the median ε_{NH3} value for the entire OWLETS-2 study

187 was 0.915, showing NH_3 partitioning was shifted towards the gas-phase.

188   The diurnal profile of aerosol pH computed using the NH_3 partitioning method followed

189   a qualitatively similar pattern to prior studies (Battaglia et al. 2017), with maxima in the early

190   morning and minima in the afternoon; however, there was a much smaller amplitude in the

191   median hourly pH values (Fig. 3). The highest median pH value (1.97) was observed between

192   07:00 – 08:00 LT, while the lowest median pH (1.50) was observed between 16:00 – 17:00 LT.

193   For the entire study, there was only a ~1 pH unit difference between the 10th and 90th percentile

194   values (1.39 and 2.36, respectively). The relatively muted diurnal profile of aerosol pH was due

195   to the unique meteorology that resembled a nearby urban site at night and transitioned to match

196   the nearby rural site during the day. The companion paper shows the diurnal profiles of aerosol

197   inorganic composition (Balasus et al., 2021). Figures 2 and 3 are consistent with recent studies

198   that demonstrate the high sensitivity of pH to meteorological factors (Battaglia et al., 2017; Tao

199   & Murphy, 2019; Zheng et al., 2020).   It is interesting to note that the ISORROPIA predictions

200   of aerosol pH yield a distinctly different diurnal profile than the pH predicted by NH_3

201   partitioning (Fig. S3). The difference in pH between the two methods peaked in the afternoon

202   between 12:00 – 14:00 LT, when particles were most acidic, and was a minimum in the early

203   morning when pH was highest (Fig. S3). The reason for these discrepancies are explored in the

204   discussion below.

205   Results suggest that pH was most sensitive to temperature changes at HMI during

206   OWLETS-2 (Fig. 4a). Across the full temperature range, the observed pH sensitivity to

207   temperature was -0.047 K^{-1}. A recent study contrasting pH in the southeast US and the North

208   China Plain found that temperature affects pH linearly at a rate of approximately -0.055 K^{-1}

209   (Zheng et al., 2020). A separate study from a Canadian observational network found that the

210   pH-temperature dependence is not linear, but changes with temperature (Tao and Murphy, 2019;

211   Tao, 2020). Over the range of conditions observed during OWLETS-2, Tao (2020) computed a

212   pH sensitivity to temperature of approximately -0.045 K^{-1} to -0.055 K^{-1}. In a previous study, the

213   pH sensitivity to temperature in Baltimore was -0.048 K^{-1}, though this was calculated for

214   conditions of constant atmospheric composition (Battaglia et al., 2017). While the present

215   results share consistencies with these studies, the results in Fig. 4a suggest important differences,

216   as well. An increase in pH was observed with increasing temperature for conditions below 293

217   K (n=156). In the companion paper, NH_3 concentrations dramatically increased with

218   temperature < 293 K but exhibited a much weaker dependence on temperature for conditions >

219   293 K (Balasus et al., 2021). Under the warmer conditions, the pH relationship with temperature

220   was linear during OWLETS-2, with a sensitivity of -0.085 K^{-1} (Fig. 4a). The results in Fig. 4a

221   are consistent with Tao (2020), as they demonstrate the offsetting responses of pH to temperature

222   through effects on NH_3 emissions and partitioning.

223   These results contribute to the growing body of work demonstrating the importance of

224   temperature to aerosol pH. Collectively, these studies suggest that the sensitivity of pH to

225   temperature is constrained between -0.045 K^{-1} and -0.085 K^{-1}, although the present results

226   illustrate circumstances where a positive relationship between temperature and pH can exist, as

227   well. It is notable that similar $\Delta pH/\Delta T$ values are observed across a range of locations and for

228   variable data sets that include monthly averages of long-term observations (Tao and Murphy,

229   2019) and 20-min measurements made over a period of weeks (presented here).

230   Aerosol pH was not strongly affected by ALWC over the range of conditions observed

231   during OWLETS-2, except at ALWC below 1 µg m^{-3} (Fig. 4b). At the lowest ALWC levels, the

232   increase in pH occurs because of the diluting effect of water, however, at ALWC above 1 µg m^{-3},

233   other factors appear to be more important (e.g., temperature). ALWC was recently identified as

234   the most significant contributor to regional pH differences (Zheng et al., 2020). In that study, the

235   pH-ALWC relationship was highly non-linear, with the greatest sensitivity calculated at ALWC

236   at levels < 25 µg m^{-3}, conditions corresponding to all the OWLETS-2 observations. Tao (2020)

237   found that pH is extremely sensitive to RH, presumed to be a surrogate for ALWC, when RH

238   was $< 20\%$ or RH $> 80\%$; however, pH was quite insensitive to RH variations in the region of

239    $20\% < RH < 80\%$. Approximately 25% (208 out of 875) of RH values during OWLETS-2 were

240   above 80%, yet no increase in pH was observed at the highest ALWC, suggesting that other

241   factors were offsetting the diluting effect of water as ALWC increased. It is interesting to note

242   that ISORROPIA predicts a stronger effect of ALWC on pH, with the diluting effect apparent as

243   pH increases with increasing ALWC. A combination of particle mass loading, aerosol

244   composition, and ambient RH are responsible for the variations in ALWC.

245   The result shown in Fig. 4b is somewhat surprising because NH$_3$ partitioning was quite

246   sensitive to ALWC (Fig. 5); the relatively invariant aerosol pH is unexpected given the increase

247   in NH$_3$ uptake in the presence of ALWC. With increasing NH$_3$ uptake in the presence of, and

248   concurrent with, the increased ALWC, it would be anticipated that aerosol pH would become

249   more basic both through the reaction of NH$_3$ to form NH$_4^+$ and due to the dilution effect of liquid

250   water. However, the results of Figures 4 and 5 reveal that despite both the increase in NH$_3$

251   uptake and increase in ALWC, aerosol pH remains relatively unchanged, with only a 0.5 pH unit

252   change at the highest values of ALWC. NH$_3$ partitioning shifted towards the condensed phase

253   (ε_{NH3} decreased) at increasing ALWC, consistent with the results of Nenes et al. (2020). ε_{NH3}

254   was more sensitive to ALWC than it was to either temp or RH (Fig. S5). This result shows the

255   importance that ALWC can have on PM$_{2.5}$ mass concentrations, as water serves as an important

256   medium enhancing the condensation of organic and inorganic water-soluble species (Carlton et

257   al., 2018; El-Sayed et al., 2016). Fig. 5 demonstrates the importance of ALWC in changing the

258   dry deposition of reactive nitrogen species. Nenes et al. (2021) predicts that NH_3 and HNO_3 dry

259   deposition rates will both be high under the conditions observed during OWLETS-2 (i.e., ALWC

260   < 10 µg m^{-3} and pH ~ 1.5). This is also consistent with a modeling study showing increased dry

261   deposition of reactive nitrogen in coastal regions, including the OWLETS-2 study domain

262   (Loughner et al., 2016).

263

264   **3.2 Composition Effects on Aerosol pH**

265   In contrast to meteorological factors, aerosol composition did not have a major effect on

266   pH variability during OWLETS-2. Consistent with prior studies, neither the sulfate

267   concentration nor the NH_4^+:SO_4^{2-} molar ratio contributed significantly to pH variability (Weber

268   et al., 2016; Hennigan et al., 2015). Fig. 4c shows that pH was also relatively insensitive to the

269   Tot-NH_3 concentration, in agreement with the results from other locations (Zheng et al., 2020;

270   Tao, 2020; Weber et al., 2016). While the predictions of ISORROPIA generally did not capture

271   the trends between pH and the meteorological factors, it is interesting to note that ISORROPIA

272   predicts that pH is relatively insensitive to Tot-NH_3, as well, except at the highest concentrations

273   (Fig. S4).

274   Composition and concentration differences between HMI and the urban and rural sites

275   are analyzed in more detail in the companion paper (Balasus et al., 2021). In the companion

276   paper, episodic NH_3 events that derived from dairy, poultry, and industrial sources were

277   characterized (Balasus et al., 2021). For the events with complete aerosol composition and

278   meteorology data (8 out of 11 NH_3 events total), mean and medial aerosol pH (2.00 and 1.96,

279   respectively) were only moderately higher than the study mean and median pH values (1.85 and

280   1.83, respectively); this difference is not statistically significant at the 95% confidence interval.

281   This includes an aerosol pH of 1.92 at the peak NH_3 concentration observed during the entire

282   study (19.3 μg m^{-3}), an event influenced by industrial emissions near downtown Baltimore

283   (Balasus et al., 2021). Together, the results suggest that pH may be more affected by the

284   proximity of the HMI site to the Chesapeake Bay than it was to regional agricultural NH_3

285   emissions, or to episodic NH_3 events from local industrial sources.

286

287   **3.3 Case Study: Effect of NVCs on pH**

288   NVCs affect thermodynamic predictions of NH_3 partitioning and thus, pH (Guo et al.,

289   2018; Vasilakos et al., 2018). Seawater is alkaline and primary marine emissions contain high

290   concentrations of NVCs (O'Dowd & De Leeuw, 2007). Marine aerosols rapidly acidify,

291   typically in seconds or minutes, though the timescale depends upon particle size (Angle et al.,

292   2021; Pszenny et al., 2004). Studies have examined the acidity of sea spray aerosols and their

293   evolution but none, to our knowledge, have done so in a polluted urban environment. The

294   OWLETS-2 study offered a unique opportunity to analyze the pH of primary marine particles

295   emitted within several km of a large urban area. The Chesapeake Bay is brackish, with

296   increasing salinity moving down the bay towards the Atlantic Ocean (Pritchard, 1952). Near the

297   OWLETS-2 measurement site at HMI, salinity is variable but average conditions are ~5 g kg^{-1}

298   (www.chesapeakebay.net, last accessed 20-November 2020). This is about a factor of seven

299   lower than typical seawater, but shows the potential for primary emissions to contribute salts that

300   could impact aerosol pH at HMI.

301   Elevated concentrations of Na^+ and Cl^- in $PM_{2.5}$ were infrequently observed during

302   OWLETS-2, with one notable 36-hour period showing evidence of primary marine impact. Na^+

303 and Cl⁻ were well-correlated ($R^2 = 0.78$) from 11-June to 13-June, a period that coincided with

304 the highest concentrations of both species (Fig. 6 and Fig. 7). It is noteworthy that wind speeds

305 were not elevated during this time (average winds = 3.1 m s⁻¹ compared to campaign-average

306 wind speeds of 2.9 m s⁻¹); longer-term measurements would be needed to characterize factors

307 driving the primary bay emissions. During this event, the pH calculation using NH_3 partitioning

308 suggests that the primary marine emissions had a minimal effect on aerosol pH. The average pH

309 during this period was 1.98, which was only slightly higher than the average for the entire study

310 (1.85). Further, as the total $Na^+ + Cl^-$ concentration increased by more than an order of

311 magnitude, from 0.05 μg m⁻³ around 18:00 LT on 11 June to 0.9 μg m⁻³ at 09:00 LT on 12 June,

312 the pH only increased by 0.1 pH unit during the same period (Fig. 6). Gas-phase NH_3 data were

313 not available for the entire NaCl event, so pH calculations were limited to the first ~20 hours.

314   The pH predictions from ISORROPIA during this period display a more significant effect

315 on aerosol pH. The average pH predicted by ISORROPIA is 3.08, which is 0.7 pH units higher

316 than the study average from ISORROPIA. Further, while the pH calculated using NH_3

317 partitioning is insensitive to Na^+ and Cl⁻, ISORROPIA predicts a rise of 1.4 pH units as Na^+ and

318 Cl⁻ increase (Figure 6). The NH_3 partitioning predicted by ISORROPIA deviates from the

319 observations during this event (r = -0.19, Fig. S6). The most likely explanation for this behavior

320 is different chemical compositions of the coarse- and fine-mode particles. Fresh marine

321 emissions acidify quickly, and evidence was found for chemical processing of NaCl. HNO_3

322 displacement of HCl is a well-known phenomenon in sea salt particles (Brimblecombe & Clegg,

323 1988). Cl⁻:Na^+ ratios slightly above unity were observed when aerosol nitrate concentrations

324 were low, and below unity when nitrate concentrations were elevated (Fig. 7). Nitrate formation,

325 including HNO_3 uptake to sea salt, is highly sensitive to pH (Kakavas et al., 2021; Vasilakos et

326   al., 2018). Nitrate (along with Na^+ and Cl^-) are direct inputs to ISORROPIA, suggesting that the

327   pH trend in Fig. 6 is due to the increased influence of coarse-mode particles. The PILS inlet was

328   equipped with a 2.5 µm cut-point cyclone (URG-2000-30-EH, URG Corp.), which allows some

329   penetration of particles with d_p < 4.5 µm (http://www.urgcorp.com/products/inlets/teflon-coated-

330   [aluminum-cyclones/urg-2000-30eh](http://www.urgcorp.com/products/inlets/teflon-coated-aluminum-cyclones/urg-2000-30eh), last accessed 29 January 2021). Likewise, primary sea salt

331   emissions often exhibit a size distribution tail that extends below 2.5 µm (Feng et al., 2017).

332   The above analysis identifies limitations computing aerosol pH with both approaches and

333   highlights opportunities to use complementary information from each to inform factors driving

334   aerosol pH. ISORROPIA's assumption of an internally mixed aerosol distribution cannot be

335   applied to predict pH in this system (Fountoukis and Nenes, 2007). However, it does provide

336   insight into the likely presence of coarse mode particles with pH significantly higher than the

337   fine mode. Conversely, Na^+, Cl^- and NO_3^- are not direct inputs into the pH calculation using

338   NH_3 partitioning, though they are used to compute aerosol liquid water, which is an input in the

339   pH calculation (Zheng et al., 2020). These NVCs have been shown to have sometimes

340   significant effects on the ratios of ammonium-to-sulfate, which could lead to inconsistencies in

341   the calculation of aerosol pH when considered in the ALWC calculation only (Guo et al. 2015).

342   NH_4^+ resides predominantly in the fine mode (Seinfeld & Pandis, 2016), so the partitioning

343   approach is unlikely to capture the acidity of the coarse mode or fine-mode particles in the tail of

344   the distribution of primary emissions that may be externally mixed with secondary particles, such

345   as dust or sea salt. This may lead to underestimates of NVC effects on aerosol pH using the

346   partitioning approach. The combined information from both methods suggests that aerosols

347   sampled at HMI during the NaCl event were characterized by a strong size-dependent pH

348   gradient, with fine-mode particles more acidic (pH ~2) than the coarse mode (pH up to 4.5).

349 Estimates of pH derived from size-segregated aerosol composition measurements have observed

350 the same phenomenon (Angle et al., 2021; Fang et al., 2017; Kakavas et al., 2021; Keene et al.,

351 2002).

352

353 **4 Conclusions**

354 There is growing recognition of the importance of aerosol pH affecting atmospheric

355 processes relevant to public health and ecosystems (Fang et al., 2017; Nenes et al., 2021).

356 Observations of spatial and temporal variations in pH are needed so that the factors that control

357 pH and contribute to variability in different environments can be fully understood. This study is

358 unique as it represents the first characterization of aerosol pH at a land-water transition site near

359 a large urban area. Baltimore, MD, is impacted by regional agricultural emissions and by

360 industrial point-source emissions of NH_3. The companion paper examines the sources of

361 episodic NH_3 events and the associated effects on aerosol composition (Balasus et al., 2021).

362 Although average and peak NH_3 concentrations during this study were significantly higher than a

363 nearby inland site, the effects on aerosol pH appear relatively insignificant, as pH during the

364 peak events was only ~0.1 pH unit higher than non-event periods. This finding is consistent with

365 studies at other locations that show aerosol pH is often insensitive to Tot-NH_3 and to the aerosol

366 NH_4:SO_4 ratio (Weber et al., 2016; Zheng et al., 2020; Tao and Murphy, 2019).

367 The unique characteristics of the OWLETS-2 study and measurement locations also

368 offered insight into the composition and meteorological influences on aerosol pH. In the

369 companion paper, the composition effects were shown to be muted in comparison to the

370 meteorological effects (Balasus et al., 2021). It was shown that the unique diurnal profiles,

371 particularly in ALWC (which did not correlate with RH) and ε_{NH3} (which did not correlate with

372   T) resulted in meteorological factors, notably temperature, having the most important influence

373   on aerosol pH. Across the full temperature range of the study, the observed pH sensitivity to

374   temperature was -0.047 K^{-1}, with increases in sensitivity up to -0.085 K^{-1} when the temperature

375   was > 293 K. The sensitivity of aerosol pH shown here is in good agreement with previous

376   studies in the Baltimore region and beyond, *e.g.* Toronto (Tao and Murphy, 2019; Battaglia et al.

377   2017). Conversely, aerosol pH was not strongly affected by ALWC during the OWLETS-2

378   study, except when ALWC was below 1 $\mu g\ m^{-3}$, in contrast to the results of Zheng et al. (2020).

379   These results of Zheng et al. (2020) in identifying ALWC as the most important factor driving

380   aerosol pH variability were derived from the results of studies in multiple locations, including

381   bulk aqueous solutions. However, this analysis suggests that the factors that drive aerosol pH

382   variability may exhibit important site-to-site differences that must be considered before

383   generalizations are applied.

384   A case study of the NVC effect on aerosol pH had significantly different outcomes

385   depending on the method for calculating pH. ISORROPIA predicted a pH increase of ~ 1.4 pH

386   units during an event with primary aerosol emissions from the Chesapeake Bay, while the pH

387   calculation using NH_3 partitioning predicted a much less significant effect (~0.1 pH unit). This

388   difference is attributed to the likely presence of externally mixed particles during the events,

389   which may include primary marine emissions elevated in NVCs. Bougiatioti et al. (2016)

390   evaluated aerosol pH at a remote site in the Mediterranean, where samples with a marine origin

391   demonstrated vastly different pH between fine (avg. pH = 0.4) and coarse mode (average pH =

392   7.3) particles. Similarly, Keene et al. (2002) demonstrated the effect of marine aerosol size

393   distribution on aerosol pH, with fine mode particles predicted to reside in the range of 1-2, with

394   super-μm particles to reside in the range of 3-4, consistent with the current results. Hence, a

395   limitation of this study is the lack of size-resolved aerosol composition measurements. This

396   study underscores the need to evaluate assumptions of internally mixed aerosols when applying

397   pH calculations, which may be a critical factor in overestimating the effects of NVCs on pH.

398   Models with size-resolved aerosol composition may be required to capture this effect across

399   scales in future studies (Kakavas et al., 2021).

400

401 **Data Availability**

402   Data are available at https://www-air.larc.nasa.gov/cgi-bin/ArcView/owlets.2018.

403

404 **Supplement**

405 Supplemental Information is available for this article at:

406

407 **Acknowledgements**

408   Annmarie G. Carlton and Christopher J. Hennigan acknowledge funding from the National Science

409   Foundation, AGS-1719252 and AGS-1719245. Ruben Delgado and Vanessa Caicedo acknowledge

410   support by the Maryland Department of the Environment (contract no. U00P8400651). Nicholas Balasus

411   and Katherine Ball received support through the NOAA Office of Education, Educational Partnership

412   Program with Minority Serving Institutions (EPP/MSI) and the Cooperative Science Center for Earth

413   System Sciences and Remote Sensing Technologies (grant no. NA16SEC4810008).

414 **Author Contributions**

415   CH, AC, and RD conceived the analysis and study participation. MB, NB, and KB collected and

416   analyzed the PILS-IC and NH_3 data. NB, MB, and CH conducted the thermodynamic modeling

417   analyses. VC and AC provided analytical input and interpretation. NB, CH, KB, and MB wrote

418   the manuscript. All authors provided feedback and revisions to the manuscript.

419

Competing Interests

The authors declare they have no conflict of interest.

422 **Figures**

423

424
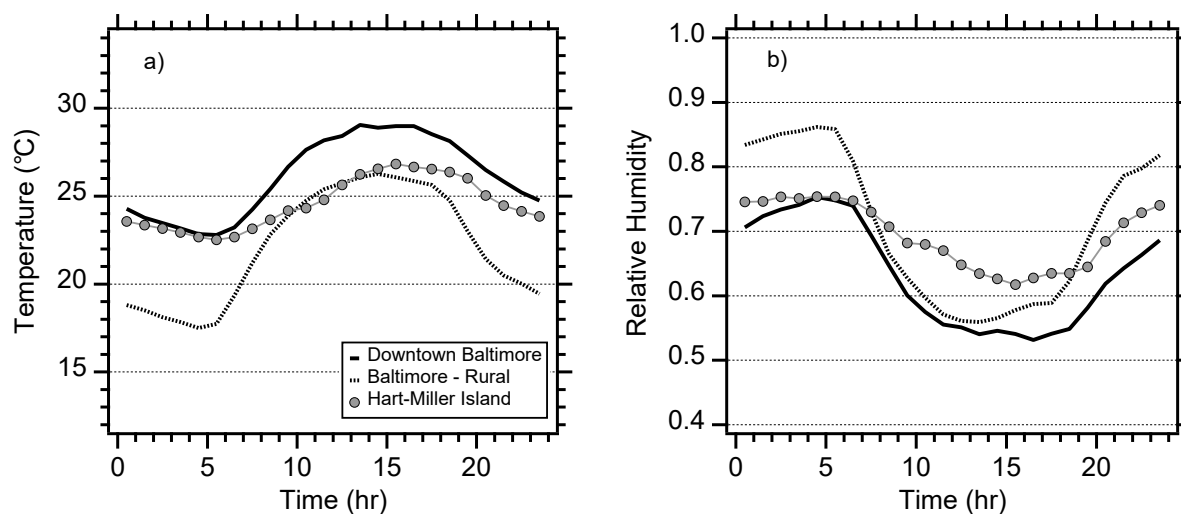
425 **Figure 1:** Diurnal profiles of (a) temperature and (b) relative humidity at three sites during the

426 OWLETS-2 study. Hart-Miller Island (HMI) is a land-water transition site and was the location

427 of aerosol composition and gas-phase measurements during the campaign. Temperatures at HMI

428 resembled the downtown location during the night but showed characteristics of the rural site

429 during the day. RH at HMI was between the urban and rural sites at night but was elevated

430 during the daytime due to the Chesapeake Bay.

431
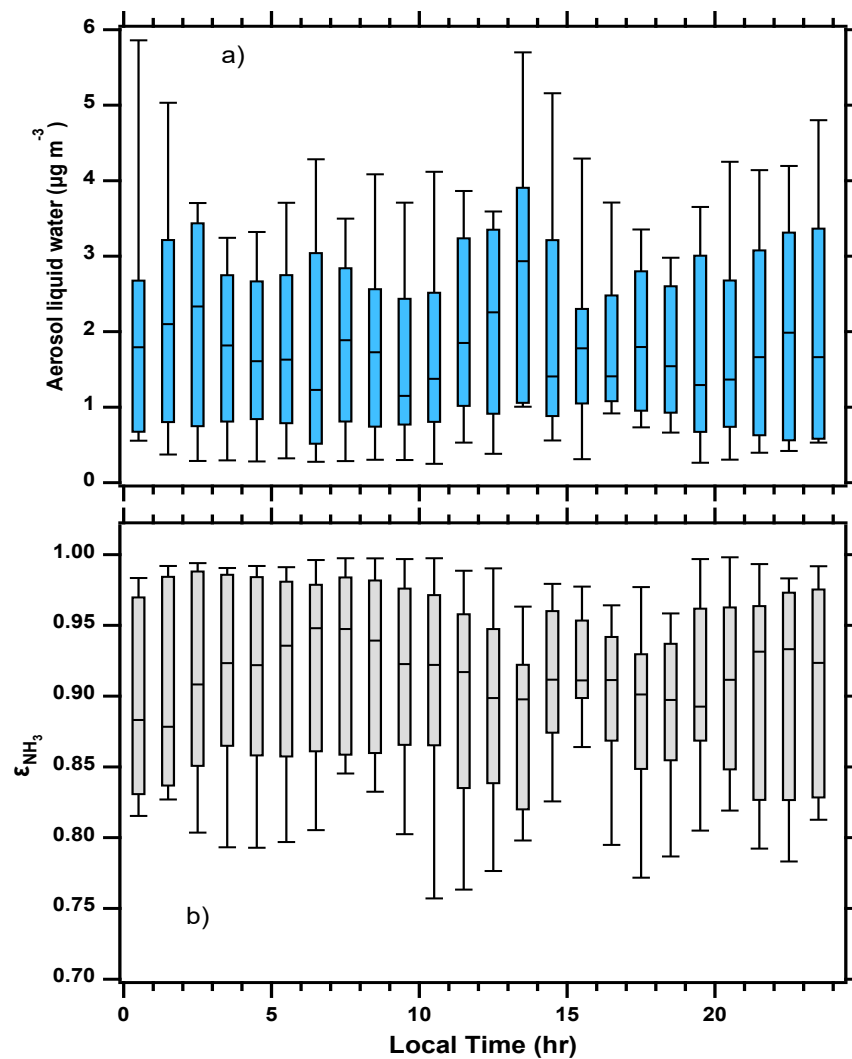
Figure 2: Box plots of (a) aerosol liquid water and (b) ε_{NH3} (ε_{NH3} = $NH_3(g)/(NH_3(g) + NH_4^+(aq))$)

during the OWLETS-2 study. The statistics shown are the median, quartiles, 10th and 90th

percentiles.

435
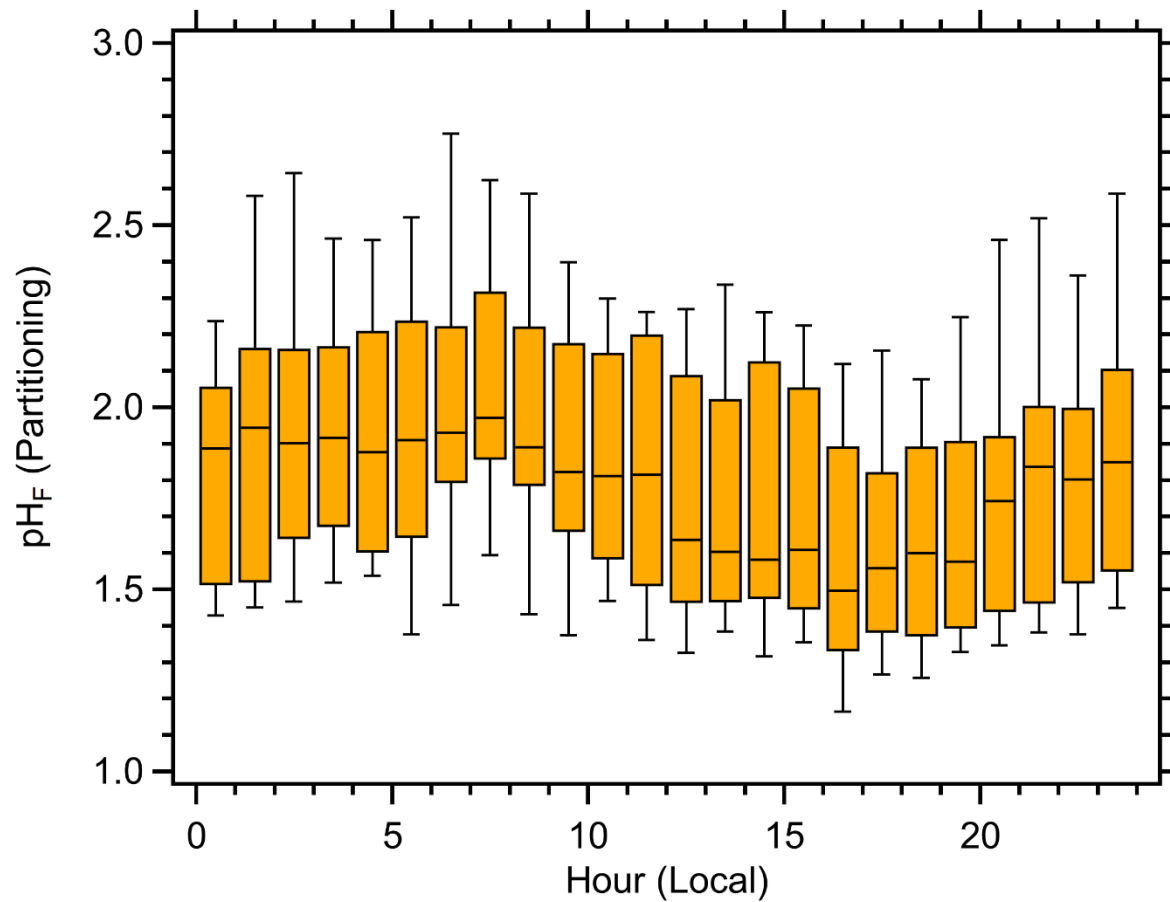
Figure 3: Box plot of the aerosol pH diurnal profile calculated using the NH_3 partitioning

method of at Hart-Miller Island during OWLETS-2. The statistics shown are the median,

quartiles, 10th and 90th percentiles.
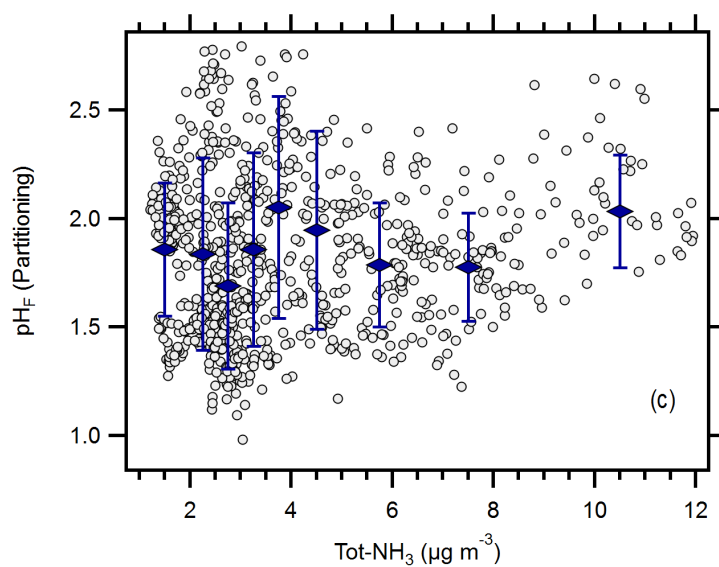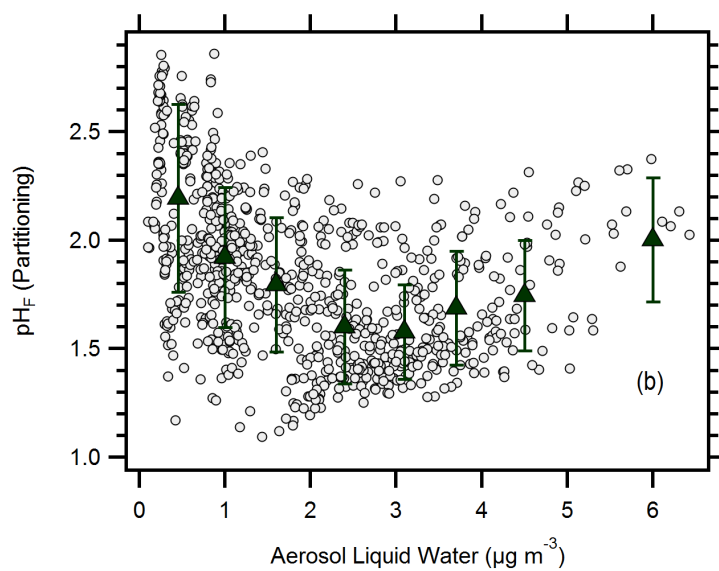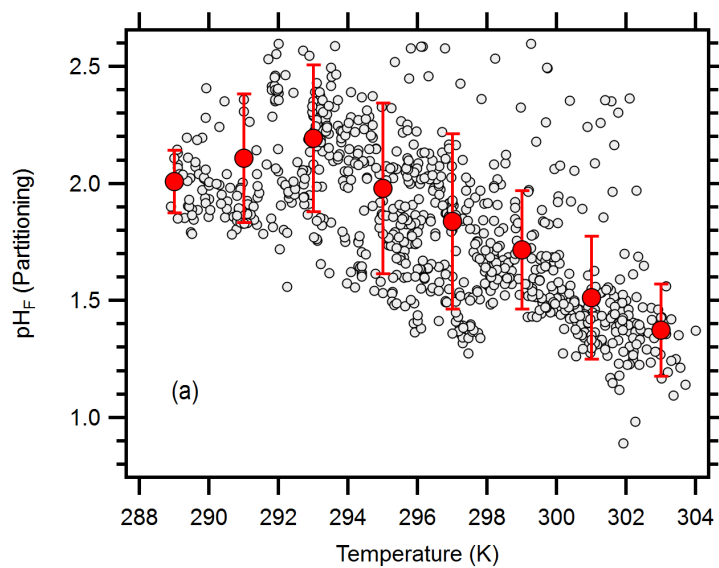
440 **Figure 4:** Relationship between aerosol pH and (a) temperature, (b) aerosol liquid water, and (c)

441 total NH_3 (Tot-NH_3 = NH_3 + NH_4^+). Symbols represent mean values while error bars represent

442 standard deviations; bins were limited to a maximum of 160 points per bin.

443
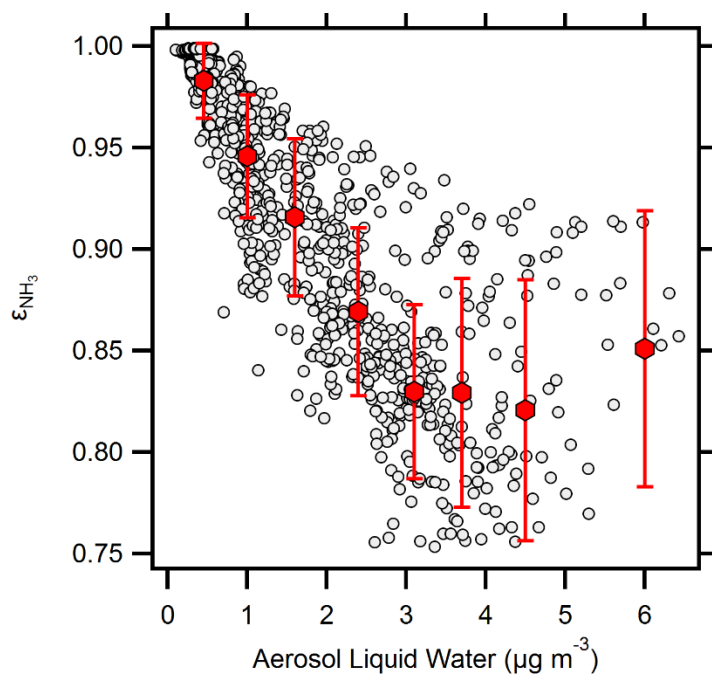
Figure 5: Relationship between NH_3 partitioning (ε_{NH3} = $NH_3/(NH_3 + NH_4^+)$) and aerosol liquid

water. Symbols represent mean values while error bars represent standard deviations; bins were

limited to a maximum of 160 points per bin.

447

448
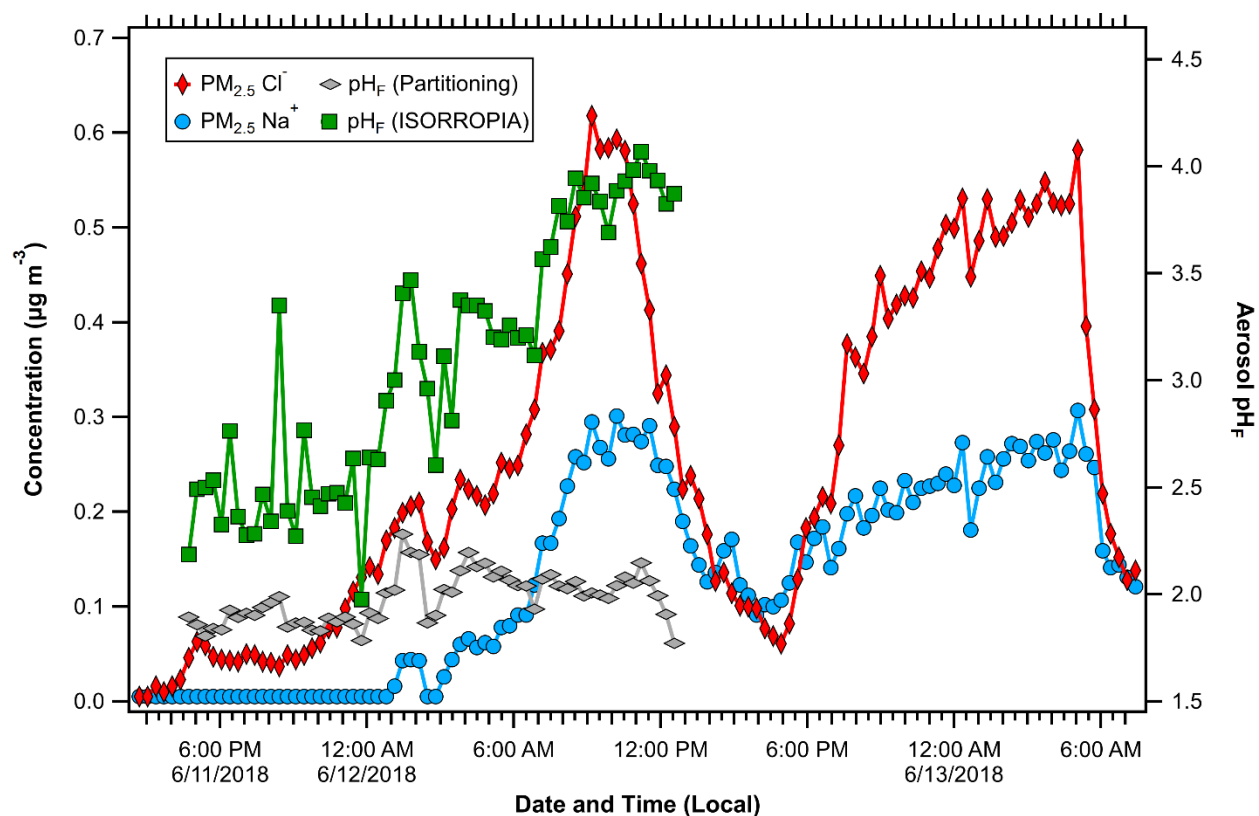
449 **Figure 6:** Concentrations of $PM_{2.5}$ Na^+ and Cl^- during a period with primary Chesapeake Bay

450 emissions. Aerosol pH calculated by NH_3 partitioning and ISORROPIA show different

451 behaviors, suggesting the aerosol distribution was externally mixed during this time.

452
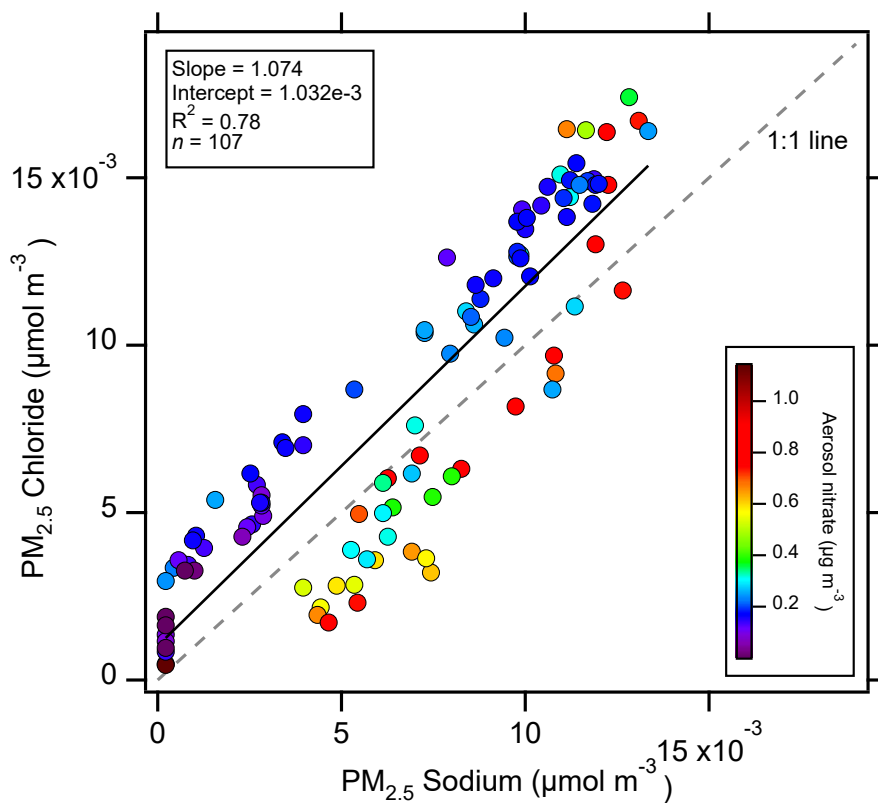
Figure 7: Correlation between PM$_{2.5}$ Na$^+$ and Cl$^-$ during the event shown in Figure 6. Lower

Cl$^-$:Na$^+$ ratios were observed at higher NO$_3^-$ concentrations, suggesting HNO$_3$ uptake displaced

HCl.

References

Angle, K. J., Crocker, D. R., Simpson, R. M. C., Mayer, K. J., Garofalo, L. A., Moore, A. N., Garcia, S. L. M., Or, V. W., Srinivasan, S., Farhan, M., Sauer, J. S., Lee, C., Pothier, M. A., Farmer, D. K., Martz, T. R., Bertram, T. H., Cappa, C. D., Prather, K. A., & Grassian, V. H. (2021). Acidity across the interface from the ocean surface to sea spray aerosol. *Proceedings of the National Academy of Sciences of the United States of America*, *118*(2), Article e2018397118. https://doi.org/10.1073/pnas.2018397118

Balasus, N., Battaglia Jr, M. A., Ball, K., Caicedo, V., Delgado, R., Carlton, A. G., & Hennigan, C. J. (2021). Urban aerosol chemistry at a land–water transition site during summer – Part 1: Impact of agricultural and industrial ammonia emissions. *Atmos. Chem. Phys.*, *21*(17), 13051-13065. https://doi.org/10.5194/acp-21-13051-2021

Battaglia Jr, M. A., Weber, R. J., Nenes, A., & Hennigan, C. J. (2019). Effects of water-soluble organic carbon on aerosol pH. *Atmos. Chem. Phys.*, *19*(23), 14607-14620. https://doi.org/10.5194/acp-19-14607-2019

Battaglia, M. A., Douglas, S., & Hennigan, C. J. (2017). Effect of the Urban Heat Island on Aerosol pH. *Environ. Sci. Technol.*, *51*(22), 13095-13103. https://doi.org/10.1021/acs.est.7b02786

Bougiatioti, A., Nikolaou, P., Stavroulas, I., Kouvarakis, G., Weber, R., Nenes, A., Kanakidou, M., & Mihalopoulos, N. (2016). Particle water and pH in the eastern Mediterranean: source variability and implications for nutrient availability. *Atmos. Chem. Phys.*, *16*(7), 4579-4591. https://doi.org/10.5194/acp-16-4579-2016

Boyer, H. C., Gorkowski, K., & Sullivan, R. C. (2020). In Situ pH Measurements of Individual Levitated Microdroplets Using Aerosol Optical Tweezers. *Analytical Chemistry*, *92*(1), 1089-1096. https://doi.org/10.1021/acs.analchem.9b04152

Brimblecombe, P., & Clegg, S. L. (1988). The Solubility and Behavior of Acid Gases in the Marine Aerosol. *Journal of Atmospheric Chemistry*, *7*(1), 1-18. https://doi.org/10.1007/bf00048251

Carlton, A. M. G., Pye, H. O. T., Baker, K. R., & Hennigan, C. J. (2018). Additional benefits of federal air quality rules: model estimates of controllable biogenic secondary organic aerosol. *Environmental Science & Technology*. https://doi.org/10.1021/acs.est.8b01869

Craig, R. L., Peterson, P. K., Nandy, L., Lei, Z., Hossain, M. A., Camarena, S., Dodson, R. A., Cook, R. D., Dutcher, C. S., & Ault, A. P. (2018). Direct Determination of Aerosol pH: Size-Resolved Measurements of Submicrometer and Supermicrometer Aqueous Particles. *Analytical Chemistry*, *90*(19), 11232-11239. https://doi.org/10.1021/acs.analchem.8b00586

El-Sayed, M. M. H., Amenumey, D., & Hennigan, C. J. (2016). Drying-Induced Evaporation of Secondary Organic Aerosol during Summer. *Environmental Science & Technology*, *50*(7), 3626-3633. https://doi.org/10.1021/acs.est.5b06002

Fang, T., Guo, H. Y., Zeng, L. H., Verma, V., Nenes, A., & Weber, R. J. (2017). Highly Acidic Ambient Particles, Soluble Metals, and Oxidative Potential: A Link between Sulfate and Aerosol Toxicity. *Environmental Science & Technology*, *51*(5), 2611-2620. https://doi.org/10.1021/acs.est.6b06151

495 Feng, L., Shen, H., Zhu, Y., Gao, H., & Yao, X. (2017). Insight into Generation and Evolution of Sea-Salt
496   Aerosols from Field Measurements in Diversified Marine and Coastal Atmospheres. *Scientific*
497   *Reports*, *7*, Article 41260. https://doi.org/10.1038/srep41260

498 Fountoukis, C., & Nenes, A. (2007). ISORROPIA II: a computationally efficient thermodynamic
499   equilibrium model for K^+-Ca^{2+}-Mg^{2+}-NH_4^+-Na^+-SO_4^{2-}-NO_3^--Cl^--H_2O aerosols. *Atmos. Chem.*
500   *Phys.*, *7*(17), 4639-4659. https://doi.org/10.5194/acp-7-4639-2007

501 Guo, H., Liu, J., Froyd, K. D., Roberts, J. M., Veres, P. R., Hayes, P. L., Jimenez, J. L., Nenes, A., &
502   Weber, R. J. (2017). Fine particle pH and gas–particle phase partitioning of inorganic species in
503   Pasadena, California, during the 2010 CalNex campaign. *Atmos. Chem. Phys.*, *17*(9), 5703-5719.
504   https://doi.org/10.5194/acp-17-5703-2017

505 Guo, H., Nenes, A., & Weber, R. J. (2018). The underappreciated role of nonvolatile cations in aerosol
506   ammonium-sulfate molar ratios. *Atmos. Chem. Phys.*, *18*(23), 17307-17323.
507   https://doi.org/10.5194/acp-18-17307-2018

508 Guo, H., Xu, L., Bougiatioti, A., Cerully, K. M., Capps, S. L., Hite, J. R., Carlton, A. G., Lee, S. H.,
509   Bergin, M. H., Ng, N. L., Nenes, A., & Weber, R. J. (2015). Fine-particle water and pH in the
510   southeastern United States. *Atmos. Chem. Phys.*, *15*(9), 5211-5228. https://doi.org/10.5194/acp-
511   15-5211-2015

512 He, H., Stehr, J. W., Hains, J. C., Krask, D. J., Doddridge, B. G., Vinnikov, K. Y., Canty, T. P., Hosley,
513   K. M., Salawitch, R. J., Worden, H. M., & Dickerson, R. R. (2013). Trends in emissions and
514   concentrations of air pollutants in the lower troposphere in the Baltimore/Washington airshed
515   from 1997 to 2011. *Atmospheric Chemistry and Physics*, *13*(15), 7859-7874.
516   https://doi.org/10.5194/acp-13-7859-2013

517 Hennigan, C. J., Izumi, J., Sullivan, A. P., Weber, R. J., & Nenes, A. (2015). A critical evaluation of
518   proxy methods used to estimate the acidity of atmospheric particles. *Atmos. Chem. Phys.*, *15*(5),
519   2775-2790. https://doi.org/10.5194/acp-15-2775-2015

520 Jang, M., Sun, S., Winslow, R., Han, S., & Yu, Z. (2020). In situ aerosol acidity measurements using a
521   UV–Visible micro-spectrometer and its application to the ambient air. *Aerosol Science and*
522   *Technology*, *54*(4), 446-461. https://doi.org/10.1080/02786826.2020.1711510

523 Kakavas, S., Patoulias, D., Zakoura, M., Nenes, A., & Pandis, S. N. (2021). Size-resolved aerosol pH
524   over Europe during summer. *Atmos. Chem. Phys.*, *21*(2), 799-811. https://doi.org/10.5194/acp-21-
525   799-2021

526 Kanakidou, M., Myriokefalitakis, S., Daskalakis, N., Fanourgakis, G., Nenes, A., Baker, A. R., Tsigaridis,
527   K., & Mihalopoulos, N. (2016). Past, Present, and Future Atmospheric Nitrogen Deposition. *J.*
528   *Atmos. Sci.*, *73*(5), 2039-2047. https://doi.org/10.1175/jas-d-15-0278.1

529 Keene, W. C., Pszenny, A. A. P., Maben, J. R., & Sander, R. (2002). Variation of marine aerosol acidity
530   with particle size. *Geophysical Research Letters*, *29*(7), Article 1101.
531   https://doi.org/10.1029/2001gl013881

532 Keene, W. C., Pszenny, A. A. P., Maben, J. R., Stevenson, E., & Wall, A. (2004). Closure evaluation of
533   size-resolved aerosol pH in the New England coastal atmosphere during summer. *J. Geophys.*
534   *Res.-Atmos.*, *109*(D23), D23307, Article D23307. https://doi.org/10.1029/2004jd004801

535 Loughner, C. P., Tzortziou, M., Follette-Cook, M., Pickering, K. E., Goldberg, D., Satam, C.,
536    Weinheimer, A., Crawford, J. H., Knapp, D. J., Montzka, D. D., Diskin, G. S., & Dickerson, R.
537    R. (2014). Impact of Bay-Breeze Circulations on Surface Air Quality and Boundary Layer
538    Export. *Journal of Applied Meteorology and Climatology*, *53*(7), 1697-1713.
539    https://doi.org/10.1175/jamc-d-13-0323.1

540 Loughner, C. P., Tzortziou, M., Shroder, S., & Pickering, K. E. (2016). Enhanced dry deposition of
541    nitrogen pollution near coastlines: A case study covering the Chesapeake Bay estuary and
542    Atlantic Ocean coastline. *Journal of Geophysical Research-Atmospheres*, *121*(23), 14221-14238.
543    https://doi.org/10.1002/2016jd025571

544 Murphy, J. G., Gregoire, P., Tevlin, A., Wentworth, G., Ellis, R., Markovic, M., & VandenBoer, T.
545    (2017). Observational constraints on particle acidity using measurements and modelling of
546    particles and gases [10.1039/C7FD00086C]. *Faraday Discussions*.
547    https://doi.org/10.1039/C7FD00086C

548 Nenes, A., Pandis, S. N., Kanakidou, M., Russell, A. G., Song, S., Vasilakos, P., & Weber, R. J. (2021).
549    Aerosol acidity and liquid water content regulate the dry deposition of inorganic reactive
550    nitrogen. *Atmos. Chem. Phys.*, *21*(8), 6023-6033. https://doi.org/10.5194/acp-21-6023-2021

551 Nenes, A., Pandis, S. N., Weber, R. J., & Russell, A. (2020). Aerosol pH and liquid water content
552    determine when particulate matter is sensitive to ammonia and nitrate availability. *Atmos. Chem.*
553    *Phys.*, *20*(5), 3249-3258. https://doi.org/10.5194/acp-20-3249-2020

554 Norman, M., Spirig, C., Wolff, V., Trebs, I., Flechard, C., Wisthaler, A., Schnitzhofer, R., Hansel, A., &
555    Neftel, A. (2009). Intercomparison of ammonia measurement techniques at an intensively
556    managed grassland site (Oensingen, Switzerland). *Atmospheric Chemistry and Physics*, *9*(8),
557    2635-2645. <Go to ISI>://WOS:000265743100002

558 O'Dowd, C. D., & De Leeuw, G. (2007). Marine aerosol production: a review of the current knowledge.
559    *Philosophical Transactions of the Royal Society a-Mathematical Physical and Engineering*
560    *Sciences*, *365*(1856), 1753-1774. https://doi.org/10.1098/rsta.2007.2043

561 Phillips, S. M., Bellcross, A. D., & Smith, G. D. (2017). Light Absorption by Brown Carbon in the
562    Southeastern United States is pH-dependent. *Environmental Science & Technology*.
563    https://doi.org/10.1021/acs.est.7b01116

564 Pinder, R. W., Adams, P. J., Pandis, S. N., & Gilliland, A. B. (2006). Temporally resolved ammonia
565    emission inventories: Current estimates, evaluation tools, and measurement needs. *Journal of*
566    *Geophysical Research-Atmospheres*, *111*(D16), Article D16310.
567    https://doi.org/10.1029/2005jd006603

568 Pritchard, D. W. (1952). Salinity Distribution and Circulation in the Chesapeake Bay Estuarine System.
569    *Journal of Marine Research*, *11*(2), 106-123. <Go to ISI>://WOS:A1952XR64900002

570 Pszenny, A. A. P., Moldanov, J., Keene, W. C., Sander, R., Maben, J. R., Martinez, M., Crutzen, P. J.,
571    Perner, D., & Prinn, R. G. (2004). Halogen cycling and aerosol pH in the Hawaiian marine
572    boundary layer. *Atmospheric Chemistry and Physics*, *4*, 147-168. https://doi.org/10.5194/acp-4-
573    147-2004

574   Pye, H. O. T., Nenes, A., Alexander, B., Ault, A. P., Barth, M. C., Clegg, S. L., Collett Jr, J. L., Fahey, K.
575   M., Hennigan, C. J., Herrmann, H., Kanakidou, M., Kelly, J. T., Ku, I. T., McNeill, V. F.,
576   Riemer, N., Schaefer, T., Shi, G., Tilgner, A., Walker, J. T., Wang, T., Weber, R., Xing, J.,
577   Zaveri, R. A., & Zuend, A. (2020). The acidity of atmospheric particles and clouds. *Atmos. Chem.*
578   *Phys.*, *20*(8), 4809-4888. https://doi.org/10.5194/acp-20-4809-2020

579   Pye, H. O. T., Zuend, A., Fry, J. L., Isaacman-VanWertz, G., Capps, S. L., Appel, K. W., Foroutan, H.,
580   Xu, L., Ng, N. L., & Goldstein, A. H. (2018). Coupling of organic and inorganic aerosol systems
581   and the effect on gas–particle partitioning in the southeastern US. *Atmos. Chem. Phys.*, *18*(1),
582   357-370. https://doi.org/10.5194/acp-18-357-2018

583   Rindelaub, J. D., Craig, R. L., Nandy, L., Bondy, A. L., Dutcher, C. S., Shepson, P. B., & Ault, A. P.
584   (2016). Direct Measurement of pH in Individual Particles via Raman Microspectroscopy and
585   Variation in Acidity with Relative Humidity. *J. Phys. Chem. A*, *120*(6), 911-917.
586   https://doi.org/10.1021/acs.jpca.5b12699

587   Seinfeld, J. H., & Pandis, S. N. (2016). *Atmospheric chemistry and physics: from air pollution to climate*
588   *change* (3 ed.). John Wiley & Sons.

589   Tao, Y. (2020). *Identification of Major Factors Influencing Aerosol pH and the Quantitative Relationship*
590   *between pH and Ammonia Gas/Particle Partitioning* University of Toronto]. University of
591   Toronto TSpace. https://hdl.handle.net/1807/103788

592   Tao, Y., & Murphy, J. G. (2019). The sensitivity of PM2.5 acidity to meteorological parameters and
593   chemical composition changes: 10-year records from six Canadian monitoring sites. *Atmos.*
594   *Chem. Phys.*, *19*(14), 9309-9320. https://doi.org/10.5194/acp-19-9309-2019

595   Valerino, M. J., Johnson, J. J., Izumi, J., Orozco, D., Hoff, R. M., Delgado, R., & Hennigan, C. J. (2017).
596   Sources and composition of PM2.5 in the Colorado Front Range during the DISCOVER-AQ
597   study. *Journal of Geophysical Research-Atmospheres*, *122*(1), 566-582.
598   https://doi.org/10.1002/2016jd025830

599   Vasilakos, P., Russell, A., Weber, R., & Nenes, A. (2018). Understanding nitrate formation in a world
600   with less sulfate. *Atmos. Chem. Phys.*, *18*(17), 12765-12775. https://doi.org/10.5194/acp-18-
601   12765-2018

602   Weber, R. J., Guo, H., Russell, A. G., & Nenes, A. (2016). High aerosol acidity despite declining
603   atmospheric sulfate concentrations over the past 15 years [Letter]. *Nature Geoscience*, *9*(4), 282-
604   285. https://doi.org/10.1038/ngeo2665

605   Zheng, G., Su, H., Wang, S., Andreae, M. O., Pöschl, U., & Cheng, Y. (2020). Multiphase buffer theory
606   explains contrasts in atmospheric aerosol acidity. *Science*, *369*(6509), 1374.
607   https://doi.org/10.1126/science.aba3719

608